

Beyond conventional wisdom: unveiling quantitative insights in fluorescence lifetime imaging via realistic simulation of biological systems

Pingchuan Ma^{1,2} and Yao Chen^{1,*}

1. Department of Neuroscience, Washington University in St. Louis, St. Louis, MO 63110
2. Ph.D. Program in Neuroscience, Washington University in St. Louis

*Corresponding author. Email: yaochen@wustl.edu

Abstract

Fluorescence lifetime imaging microscopy (FLIM) and photometry (FLiP) are illuminating the dynamics of biological signals. Because fluorescence lifetime is an intensive property of a fluorophore that is insensitive to sensor expression levels, it excels over fluorescence intensity measurements by allowing comparison across animals, over chronic time periods, and quantitation of the absolute levels of biological signals. However, the insensitivity of lifetime to sensor expression level does not always hold true in biological experiments where autofluorescence, ambient light, dark currents and afterpulses of the detectors are present. To quantitatively evaluate the potential and limitations of fluorescence lifetime measurements, we introduce FLiSimBA, a flexible platform enabling realistic Fluorescence Lifetime Simulation for Biological Applications. FLiSimBA accurately recapitulates experimental data and provides quantitative analyses. Using FLiSimBA, we determine the photons required for minimum detectable differences in lifetime and quantify the impact of hardware innovation. Furthermore, we challenge the conventional view that fluorescence lifetime is insensitive to sensor expression levels and define the conditions in which sensor express levels do not result in statistically significant difference in biological experiments. Thus, we introduce an adaptable simulation tool that allows systematic exploration of parameters to define experimental advantages and limitations in biological applications. Moreover, we provide a statistical framework and quantitative insights into the impact of key experimental parameters on signal-to-noise ratio and fluorescence lifetime responses. Our tool and results will enable the growing community of FLIM users and developers to optimize FLIM experiments, expose limitations, and identify opportunities for future innovation of fluorescence lifetime technologies.

Introduction

Fluorescence lifetime imaging microscopy (FLIM) and photometry (FLiP) are powerful methods to reveal the dynamics of biological signals^{1–18}. Fluorescence lifetime refers to the time between excitation of a fluorophore and emission of light. Compared with intensity-based imaging, the biggest advantage of fluorescence lifetime comes from its insensitivity to fluorophore concentration. As a result, fluorescence lifetime can be used to compare the dynamics of biological signals across animals or over long periods of time despite sensor expression level change. Furthermore, it offers the potential to quantitate absolute values of biological signals because of its quantitative nature and its insensitivity to sensor expression. Because of these advantages, more FLIM-compatible sensors have been developed and FLIM is increasingly adopted to elucidate the dynamics of many types of biological signals over multiple time scales.

Although fluorescence lifetime is independent of sensor expression when only the sensor is present, in biology experiments, this very advantage of FLIM breaks down when multiple other factors are present. These include autofluorescence, background light (e.g., ambient light), dark current and afterpulse of the photomultiplier tube (PMT)^{1,19–21}. As sensor expression varies, the relative contribution of sensor fluorescence and these other sources of light or electrical noise varies correspondingly, leading to an apparent change in fluorescence lifetime. Thus, to harness the power and correctly interpret results of FLIM and FLiP experiments in biological tissue, it is critical to understand quantitatively the regime when fluorescence lifetime varies with sensor expression, and the range when sensor expression does not significantly alter lifetime measurements. Furthermore, these additional factors introduce bias and noise to fluorescence lifetime measurements. As innovation pushes the technological boundary to image larger fields of view at higher speed^{22–25}, it is critical to understand how these factors contribute to signal-to-noise (SNR) ratio, and how many photons are required to achieve a certain SNR in biological settings.

An effective tool to explore how experimental parameters contribute to outcome is simulation. Both analytical and simulation methods have provided insights into issues such as SNR^{15,26–34}. However, prior work usually assumes the presence of sensor fluorescence only without considering the important contributions to noise and bias due to other factors such as autofluorescence and afterpulse of the PMT. Consequently, these simulations are useful in vitro but not readily applicable in biological settings. Therefore, to understand how experimental conditions influence lifetime estimate for biological applications, it is essential to perform simulations with realistic and, ideally, measured data.

Here we introduce Fluorescence Lifetime Simulation for Biological Applications (FLiSimBA) and use it to quantitatively define the potential and limitation of lifetime experiments in biological settings. FLiSimBA is a flexible platform designed for realistic simulation of fluorescence lifetime data through time-correlated single photon counting (TCSPC). FLiSimBA recapitulates experimental data. Using the realistically simulated histograms, we determine photon requirements for minimum detectable difference in fluorescence lifetime and assess the impact of hardware innovation on SNR. Furthermore, we challenge the conventional view that fluorescence lifetime is insensitive to sensor expression levels and establish the quantitative limits of insensitivity. Thus, we provide a versatile tool to simulate experimental conditions with empirically determined parameters. Furthermore, we provide a quantitative framework to evaluate fluorescence lifetime

results, generating insights into the potential and limitations of fluorescence lifetime measurements in biological applications.

Results

Simulation of fluorescence lifetime data in biological tissue

To realistically mimic fluorescence lifetime in biological tissue, we simulated contributions from sensor fluorescence, autofluorescence, afterpulse, background due to a small amount of light leak, and the dark current of the photon detectors. For sensor fluorescence, we sampled with replacement from an ideal distribution of photon lifetimes. In the examples in this study, we used the lifetime distribution of FLIM-compatible A Kinase Activity Reporter (FLIM-AKAR), a Förster resonance energy transfer (FRET)-based biosensor that measures the activity of protein kinase A (PKA) in a variety of biological contexts, including brain slices and freely moving animals^{6,10,13,14,35}. The fluorescence lifetime of FLIM-AKAR follows a double exponential decay defined by the following equation:

$$F(t) = F_0 * (P_1 * e^{\left(-\frac{t}{\tau_1}\right)} + P_2 * e^{\left(-\frac{t}{\tau_2}\right)}) \text{ (Equation 1),}$$

where $F(t)$ is number of photons that arrives at time t , F_0 is the number of photons at time 0, τ_1 and τ_2 are time constants corresponding to lifetime distributions of the donor fluorophore that is either free or undergoing FRET, and P_1 and P_2 are the proportion of the donor fluorophores in these two states (Fig. 1A). Following sampling, we convolved the lifetime histogram with an instrument response function (IRF) to account for instrument noise. Subsequently, we added sampled photons from an autofluorescence curve, whose distribution was determined with measurement in brain tissue. Autofluorescence lifetime histogram exhibited faster decay than FLIM-AKAR (Fig. 1A). After that, we added afterpulse of PMT, long-lasting signals from ionization of residual gas inside the PMT following a photon detection event¹⁹. Afterpulse was modelled as an even distribution with the number of photons as a fraction of sensor fluorescence. Finally, we added background fluorescence that is empirically determined from measurement. We generated 500 simulated fluorescence lifetime histograms for each P_1 and sensor photon count (see more details in Materials and Methods).

The simulated histogram closely matched experimental histogram (Fig. 1A). Following histogram generation, we used two commonly used fluorescence lifetime metrics to evaluate the simulated data: fitted P_1 after double exponential fitting of the final simulated data, or calculation of average lifetime of all photons, which we termed empirical lifetime. To quantitate how well our simulation matches experimental conditions, we calculated empirical lifetime after each of the simulation steps. Although autofluorescence biased empirical lifetime to be shorter, and background and afterpulse biased empirical lifetime to be longer, the empirical lifetime of final simulated data was not significantly different from experimental data (Fig. 1B; adjusted $p = 0.24$, final simulated data vs experimental data; $n = 500$ and 7 respectively). Thus, our simulated fluorescence lifetime data recapitulate experimental data in biologically relevant settings.

Bias and noise introduced by different sources of fluorescence

To understand how different fluorescence sources contribute to bias and noise, we analyzed fitted P_I and empirical lifetime across a range of values for simulated P_I and sensor photon counts. Autofluorescence decreased fitted P_I and empirical lifetime, consistent with the faster decay of autofluorescence compared with FLIM-AKAR sensor fluorescence (Fig. 1C-1D; $p < 0.0001$, sensor + autoF vs sensor only under all sensor photon number conditions for both fitted P_I and empirical lifetime). Afterpulse and background did not introduce significant change in fitted P_I ($p > 0.20$, final simulated data vs sensor + autoF condition for all sensor photon number conditions), consistent with consideration of the background term during the fitting procedure. However, afterpulse and background increased empirical lifetime, consistent with their presentation as even distribution across lifetime time channels with a higher mean lifetime than FLIM-AKAR (Fig. 1C-D; $p < 0.0001$, final simulated data vs sensor only for all sensor photon number conditions). These biases were less pronounced at higher sensor photon counts, which can be explained by the relatively small contribution of autofluorescence, afterpulse, and background when sensor fluorescence is high. Furthermore, as photon counts increased, the variance became smaller for both fitted P_I and empirical lifetime (Fig. 1D). Therefore, we defined quantitatively how different sources of fluorescence contribute to bias and noise (Fig. 1C-1D), and FLIM users can use these curves to specify the threshold of autofluorescence, afterpulse, background, and sensor fluorescence that are optimal for specific experimental needs.

Determination of minimum photon number requirements to achieve specific SNRs

How many photons do we need for a given FLIM experiment? Are more photons always better? More photons mean better SNR, but also lower sampling rate and reduced fields of view. How can we quantitatively find the optimal compromise among these factors? As sensor fluorescence increases, variances of both fitted P_I and empirical lifetime decrease (Fig. 1D), and the ability to detect a specific amount of fluorescence lifetime response increases. Although the number of photons required to achieve a certain amount of SNR was analyzed previously^{15,26-34}, such analysis had not been performed with consideration of biological samples in realistic experiments with autofluorescence, background, and afterpulse.

To determine the minimum number of photons required for a certain SNR, we analyzed the minimum detectable differences (MDD) of both fitted P_I and empirical lifetime with different numbers of sensor photons and repeated data samples (Fig. 2). The MDD was calculated with 80% power and 5% significance level. As sensor photons increased, MDDs decreased. As the number of repeated data samples increased, MDD also decreased. Importantly, the MDD curves provide quantitative information on the minimum number of photons required for a certain amount of expected signal. For example, to detect a P_I change of 0.006 or a lifetime change of 5ps, approximately 300,000 photons are required. As sensor fluorescence increased, the gain in signal-to-noise ratio became less and less. Thus, MDD curves generated with FLiSimBA are instrumental to determine the optimal experimental conditions (for example, optimal imaging speed and sizes of imaging fields) necessary to detect a minimum amount of lifetime change.

Impact of hardware on MDD: a comparison between gallium arsenide phosphide (GaAsP) PMTs and hybrid detectors

FLiSimBA can be used to quantitatively evaluate the benefit of specific hardware changes on SNR. Hybrid detector (HBD) is advantageous over traditional GaAsP PMT due to its narrower IRF width and lack of afterpulsing³⁶. However, hybrid detectors are more expensive. Thus, it is valuable to quantify how much benefit HBD can bring over traditional GaAsP PMTs for SNR. To answer this question, we simulated fluorescence lifetime histograms with narrower IRFs (Fig. 3A) and no afterpulse for HBD and compared them with the simulated data for traditional GaAsP PMTs. The simulation indicated that hybrid detectors and GaAsP PMTs displayed similar photon-dependent change in fitted P_I and empirical lifetime (Fig. 3B; $p < 0.01$ for fitted P_I , 800,000 photons vs majority of the photon number conditions, for both GaAsP PMT and HBD; $p < 0.05$ for empirical lifetime, 800,000 photons vs all other photon number conditions, for both GaAsP PMT and HBD). For both fitted P_I and empirical lifetime, a given sensor photon number gave a comparable MDD for HBDs and GaAsP PMTs (Fig. 3C), which can be explained by the similar levels of variance from HBD and PMT simulations (Fig. 3B). Thus, HBD with narrower IRF and low afterpulse yield little improvement on the SNR for fluorescent protein-based sensors in biological applications, although it can offer other advantages²⁶. FLiSimBA thus quantitatively defines the impact on SNR due to hardware change, allowing users to determine the appropriate tradeoff between performance improvement and price given their sensor brightness, sensor lifetime, and expected signal amplitude in specific biological applications.

Expression level dependence of fluorescence lifetime estimates

Sensor expression level often changes over days and across animals and is usually assumed not to influence lifetime estimates because fluorescence lifetime is an intensive property of fluorophores. However, this assumption is true only if the biosensor is the only contributor to fluorescence. With autofluorescence, afterpulse, and background fluorescence that are present in biological applications, the amount of sensor fluorescence relative to these contributing factors can lead to an apparent change in fluorescence lifetime estimates even if the biosensor is in the same conformational state¹. Here, we challenge the conventional view that fluorescence lifetime is independent of sensor expression and use simulation to define the range when sensor expression has negligible influence on lifetime.

We first determined how sensor expression level altered responses in fitted P_I and empirical lifetime. When P_I changed from 0.4 to 0.5, both fitted P_I and empirical lifetime increased as expected (Fig. 4A, 4C; adjusted $p < 0.0001$, $P_I = 0.4$ vs $P_I = 0.5$, under all photon number conditions for both fitted P_I and empirical lifetime). As sensor photon counts increased, there was an apparent increase in fitted P_I and decrease in empirical lifetime (Fig. 4A, 4C; $p < 0.01$, 800,000 photons vs the majority of other photon count conditions, for both fitted P_I and empirical lifetime, for both $P_I = 0.4$ and $P_I = 0.5$), consistent with the diminishing effect of autofluorescence, background, and afterpulse. For the response amplitude, as sensor photon counts increased, there was also an apparent increase in the change of fitted P_I and empirical lifetime (Fig. 4B, 4D; $p < 0.05$, 800,000 photons vs the majority of other photon counts, for both fitted P_I and empirical lifetime). The response dependence on photons eventually approached asymptotes. With the parameters used in our case study, fluorescence lifetime responses were relatively stable at sensor photon counts of 200,000 and beyond but varied with lower sensor expression level (Fig. 4B, 4D). Thus, our results challenge the widely held view that fluorescence lifetime changes are

independent of sensor expression level, and FLiSimBA can be used to define a quantitative threshold of sensor expression level to reach for users to compare lifetime responses across different sensor expression levels.

How much change in sensor expression level does not lead to significant difference in lifetime? The answer to this question depends on the sensor expression level. As sensor expression level increases, the expression change-induced apparent lifetime change becomes smaller (Fig. 4B, 4D). We therefore calculated the minimum number of sensor photons required for a certain amount of change in sensor fluorescence to have nonsignificant influence on lifetime measurements. We simulated fluorescence lifetime histograms across a range of sensor photon counts and across a range of change in sensor fluorescence levels. We determined the apparent change in lifetime introduced by change in sensor expression level (Fig. 5A, purple traces). As sensor fluorescence increased, the sensor expression-induced apparent change in lifetime decreased, consistent with relatively less contribution from autofluorescence/afterpulse/background. In addition, for each sensor photon count and for each sensor expression level change, we calculated the change in lifetime that would present as significant difference for t statistics (Fig. 5A, green traces). As sensor photons increased, the difference that would present as significant t statistics also decreased, which can be explained by the decreased variance of the data. Thus, we can use these two traces in Fig. 5A to determine the point of interception – this gives the minimum number of sensor photon counts required to tolerate a certain amount of sensor photon changes (i.e., t tests would not show statistically significant difference) (Fig. 5B). As total sensor photon numbers increased, a greater number of sensor expression difference could be tolerated not to cause statistically significant difference in lifetime measurements. Thus, this curve defines a quantitative relationship to guide biological experiments on the amount of sensor photon counts required for a certain amount of sensor expression level change.

Discussion

Here we provide a quantitative framework for analyzing fluorescence lifetime in realistic biological settings. We introduce FLiSimBA, a platform that accurately simulates fluorescence lifetime data for biological applications (Fig. 1). With FLiSimBA, we address key questions in FLIM. We determine the number of photons required for different minimum detectable differences to understand SNRs (Fig. 2). Additionally, we assess the impact of hardware changes by comparing GaAsP PMTs to hybrid detectors (Fig. 3). Moreover, we challenge the conventional view that biosensor expression levels do not affect fluorescence lifetime. We reveal how variation in sensor expression influences response amplitude (Fig. 4) and identify the amount of expression level variation that does not significantly alter fluorescence lifetime estimates (Fig. 5). In summary, our study provides valuable insights and a quantitative framework to define the power and limitations of fluorescence lifetime experiments in biological applications.

FLiSimBA is a necessary and useful tool for FLIM and FLiP experiments for a few reasons. First, it makes realistic simulations of lifetime data for biological applications. Second, it is versatile and can be easily adapted to evaluate new sensors with different lifetime constants and biophysical mechanisms, new methods of calculating fluorescence lifetime, new tissues and organisms with different amounts of autofluorescence, and new hardware modifications that can minimize dark

currents, afterpulse, or enhance other aspects of FLIM capabilities. Third, FLiSimBA and the quantitative framework we provide can precisely define the benefits and limitations of a FLIM or FLiP experiment, enabling rigorous experimental design and data interpretation.

More than providing a tool and quantitative framework, this study challenges the wildly held assumptions about the very advantage of fluorescence lifetime measurements: its insensitivity to sensor expression levels. By considering autofluorescence, afterpulse, and background photon counts in biological experiments, our results define the range where expression level alters lifetime, and where it does not result in significant lifetime change (Figs. 4-5). These analyses are critical to define the window of opportunity in which FLIM and FLiP can be used to compare biosensor measurements over chronic time periods and across animals, and to quantitate absolute levels of biological signals. Finally, our results also provide the amplitude of the error bars in fluorescence lifetime measurements due to photon sampling, a necessary quantity to interpret any FLIM and FLiP data rigorously. These results empower FLIM users to precisely evaluate the compromise between SNR, field-of-view sizes, and imaging speeds.

FLiSimBA and our quantitative platform also facilitate future innovation. Whereas our simulations showed little advantage of hybrid detectors over GaAsP PMTs in terms of SNRs, different types of hybrid detectors offer narrower IRFs at the cost of lower quantum efficiency (QE). FLiSimBA enables evaluation of the tradeoff between IRF width and QE. Additionally, hybrid detectors are more advantage for shorter fluorescence lifetimes²⁶ and FLiSimBA allows exploration of the range where they provide clear benefits in biological settings. Another avenue to innovation stems from our analysis of the effects of autofluorescence (Fig. 1). Because autofluorescence cannot be readily subtracted as background from fluorescence lifetime histograms, autofluorescence introduces bias and noise to measurements. To enhance sensitivity and resolution, correcting autofluorescence interference with hardware and software approaches, or developing brighter or red sensors, is crucial. FLiSimBA and our quantitative framework are thus instrumental to evaluate specific strategies for autofluorescence correction, as well as other technical innovations for FLIM and FLiP.

Materials and Methods

Animals

All procedures for rodent husbandry and surgery were performed following protocols approved by the Washington University Institutional Animal Care and Use Committee and in accordance with National Institutes of Health guidelines. CD-1 mice (Envigo #030) were used. The experiments were performed according to the ARRIVE guidelines³⁷.

DNA plasmid

For experimentally determined data on FLIM-AKAR, AAV-FLIM-AKAR¹⁰ (Addgene #63058) was used to express the FLIM-AKAR sensor in primary somatosensory cortex by in utero electroporation⁶.

Acute brain slice preparation

Mice at 15 to 19 days of age were anesthetized with isoflurane followed by decapitation. Their brains were rapidly dissected out and put in sucrose-based cutting solution (concentrations in mM: 75 sucrose, 2.5 KCl, 1.25 NaH₂PO₄, 25 NaHCO₃, 87 NaCl, 25 glucose, 1 MgCl₂). 300 μ m-thick coronal sections with primary somatosensory cortex were obtained with a vibratome (Leica Instruments, VT1200S) in cold sucrose-based cutting solution. After sectioning, slices were transferred to artificial cerebral spinal fluid (ACSF) (concentrations in mM: 127 NaCl, 2.5 KCl, 1.25 NaH₂PO₄, 25 NaHCO₃, 2 CaCl₂, 1 MgCl₂, and 25 glucose) and incubated at 34°C for 10 minutes for recovery. Slices were kept at room temperature in ACSF with 5% CO₂ and 95% O₂. Slices were then transferred to a microscope chamber and ACSF was perfused at a flow rate of 2-4 mL/min for imaging.

Two-Photon Fluorescence Lifetime Imaging Microscopy (2pFLIM)

2pFLIM was performed as described previously^{1,6,10}. A custom-built microscope with a mode-locked laser source (Spectra-Physics, Insight X3 operating at 80 MHz) was used. Photons were collected with fast photomultiplier tubes (PMTs, Hamamatsu, H10770PB-40). A 60X (Olympus, NA 1.1) objective was used. Image acquisition was performed with the custom-written software ScanImage^{1,10,38} in MATLAB 2012b. 920 nm was used as the excitation wavelength. Emission light was collected through a dichroic mirror (FF580-FDi01-25X36, Semrock) and a band-pass filter (FF03-525/50-25, Semrock). 128x128 pixel images were collected by frame scan at 4 Hz. The FLIM board SPC-150 (Becker and Hickl GmbH) was used, and time-correlated single photon counting was performed with 256 time channels. Photons from 20 frames were pooled for fluorescence lifetime calculation. Only healthy cells (judged by gradient contrast images) at 30-50 μ m below slice surface were selected. Each individual cell was analyzed as a region of interest (ROI). Photons from a given ROI were pooled for further analysis.

Experimental data collection, determination of parameters, and simulation

Simulation was performed in MATLAB2022a with the following steps (Fig. 1A). The parameters described below were used for this study and could be altered with our code to adapt to different biological applications. The final simulated histograms consist of IRF convolved sensor fluorescence, autofluorescence, afterpulse, and background fluorescence. The simulations were

performed with 256 time channels for each laser cycle from an 80 MHz laser. For each P_I and sensor photon number condition, simulation was repeated 500 times.

1. Generation of photon populations for sensor fluorescence

For sensor fluorescence, τ_1 and τ_2 were previously determined to be 2.14 ns and 0.69 ns respectively¹⁰. To determine the appropriate photon counts and P_I range for simulation, sensor fluorescence histogram was fitted with a modified version of Equation 1.

$$F(t) = F_0 * \left(P_1 * e^{-\frac{t}{\tau_1}} + P_2 * e^{-\frac{t}{\tau_2}} \right) \otimes IRF + F_{background} \text{ (Equation 2)}$$

where $F_{background}$ is the background fluorescence that is fitted for sensor fluorescence data, and \otimes represents convolution.

To simulate fluorescence lifetime with double exponential decay, we generated a population of photons with Equation 1 with F_0 as 1,000,000. We generated photon populations and corresponding fluorescence lifetime histograms with the P_I range from 0.4 to 0.6 with an increment of 0.01.

2. Sensor fluorescence sampling and IRF convolution

For the determination of IRF, collagen fibers from mouse tail were used for second harmonic generation with excitation light at 1050 nm. The lifetime histogram was normalized with the total photon number and used as IRF.

For sensor fluorescence sampling, a specific number of photons were randomly drawn with replacement from the corresponding population generated with the double exponential decay. The IRF convolution of the fluorescence lifetime histogram was performed: the lifetime of each photon of the sample was re-distributed along the time channels based on the probability of the IRF distribution. Following convolution, the histogram was wrapped around such that any photons whose lifetime were beyond the 12.5ns of a laser cycle were redistributed to the next cycle.

Empirically measured IRF by second harmonic generation of the mouse tail was used in all figures except for Fig. 3. For Fig. 3, the IRFs of both systems were modeled as Gaussian distribution with different Gaussian width. The mean of the Gaussian distribution (μ) was set as the peak channel of the experimental collected IRF. The full width at half maximum (FWHM) of the Gaussian IRF of the GaAsP PMT was set to match the FWHM of the experimental collected IRF (340 ps). The FWHM of the hybrid detector Gaussian IRF was set as 120 ps based on the model HPM-100-40 (Becker & Hickl)³⁶. The standard deviation (STD, σ) of the Gaussian distribution of the IRFs was determined based on the relationship with FWHM:

$$FWHM = 2\sqrt{2\ln 2} * \sigma \text{ (Equation 3).}$$

The Gaussian distribution was defined as:

$$G(t) = \frac{1}{\sigma\sqrt{2\pi}} * e^{-\frac{1}{2}\left(\frac{t-\mu}{\sigma}\right)^2} \text{ (Equation 4).}$$

The gaussian IRF was generated by normalization of $G(t)$ against the total photon counts.

3. Autofluorescence

All biological tissues exhibit autofluorescence due to different fluorescent cellular components and metabolites such as nicotinamide-adenine dinucleotide (NAD), flavins, aromatic amino acids, etc^{1,20,21}. To collect the autofluorescence of brain tissue, we imaged brain slices without sensor expression from mice at postnatal 15 to 19 days of age. After brain slicing, neurons from primary somatosensory cortex were imaged under the same imaging conditions (920 nm excitation light, 2.5 mW, 30-50 μm below slice surface, and same magnification as FLIM-AKAR imaging). The decay histograms from 19 acquisitions were averaged. The number of photons from autofluorescence contributing to autofluorescence (F_{auto}) was calculated as the average autofluorescence subtracted by the number of photons contributing to background fluorescence ($F_{background}$). Autofluorescence measurements consist of true autofluorescence together with background fluorescence (due to dark current and ambient light leak). Thus, the average autofluorescence histogram was fitted with a double exponential with background (Equation 2) to determine the τ_1 , τ_2 , P_1 , P_2 of autofluorescence as well as background fluorescence. For simulated autofluorescence, up to 10% of fluctuation was introduced to the number of photons with the random draw of an integer within the range of $F_{auto}*(1\pm 5\%)$.

For Fig. 3, autofluorescence simulation with double exponential decay was used (Equation 1). For the rest of the figures, autofluorescence lifetime were sampled from the empirical autofluorescence lifetime distribution where background was subtracted from the average autofluorescence lifetime histogram.

4. Afterpulse and background fluorescence

The afterpulse ratio of the PMT was derived from IRF histogram and the background fluorescence measurement described above. Then average photons per channel at the end of the IRF histograms, where the distribution was even across time channels. This number subtracted by the background fluorescence were used as the afterpulse. Subsequently, the ratio between the number of photons contributing to afterpulse and the total number of photons from sensor fluorescence were calculated as afterpulse ratio. This ratio was determined to be 0.32% for GaAsP PMTs.

Afterpulse and background fluorescence were simulated by sampling with replacement from an even distribution across time channels. The number of photons contributing to background fluorescence was determined from autofluorescence fitting. Up to 10% of fluctuation was introduced to the number of photons with the random draw of an integer within the range of $F_{background}*(1\pm 5\%)$. The number of photons from afterpulse were determined by the afterpulse ratio (0.32% for GaAsP PMTs and 0 for hybrid detectors) multiplied by the number of photons from sensor fluorescence.

FLIM analysis

Two metrics were used for subsequent data visualization and analysis. First, the fluorescence lifetime histograms generated from simulation or experimental data were fitted by Equation 2 with Gauss-Newton method non-linear least-square fitting algorithm. Fitted P_1 , corresponding to the proportion of slower decay (2.14 ns), was used for data visualization and analysis. Second, the empirical lifetime of all the photons were calculated as:

$$\text{empirical lifetime} = \frac{\sum(F(t)*t)}{\sum F(t)} \text{ (Equation 5),}$$

in which t is the lifetime of a specific time channel, and $F(t)$ is the photon count from that time channel. The lifetime range from 0.489 ns to 11.5 ns was used for both P_I fitting and empirical lifetime calculation.

Quantification and statistical analysis

For each simulated condition, the mean and STD of the fitted P_I or empirical lifetime of the 500 simulation repeats were calculated.

For Figs. 2 and 3, the minimum detectable difference (MDD) was calculated by:

$$MDD = z * SE(\widehat{diff}) \text{ (Equation 6),}$$

where SE refers to standard error, and \widehat{diff} is the estimated mean difference between two distributions. With a significance level of 0.05 and a power of 0.8, the z value is 2.806. which was used for the calculation in this study. Under a certain sensor photon number condition, the STD of the two metrics with different P_I condition were similar to each other. Thus, given a certain sensor photon count, the STD at a certain P_I condition (used as 0.5 in Fig. 2) was used to calculate the MDD:

$$MDD = z * \frac{\sqrt{STD^2 + STD^2}}{\sqrt{n}} = \frac{z * \sqrt{2} * STD}{\sqrt{n}} \text{ (Equation 7),}$$

where n was the number of data pairs used to analyze whether there was a significant change in fitted P_I or empirical lifetime.

For Fig. 5, to determine whether a certain amount of sensor expression-induced apparent lifetime change could be tolerated, t tests were used to compare whether there was any statistically significant difference between two distributions with the same simulated P_I but different photon numbers. The critical value of the t statistic is $z = 1.96$ for a significance level of 0.05. The equation $z * SE(\widehat{diff})$ was used to calculate the lifetime difference that would show up as statistically significant. As photon counts increased, there was an intersection where the mean lifetime difference between the two distributions became less than the difference that would reach statistical significance, and this intersection point (determined by linear interpolation of the curves plotted in log scale for both axes) was used to determine the minimum sensor photon numbers required to tolerate a specific amount of sensor fluorescence change.

Wilcoxon test was used to test the significance of the difference between two distributions.

Data and code availability

All data needed to evaluate the conclusions in the paper are present in the paper. The MATLAB functions for simulation are deposited at https://github.com/YaoChenLabWashU/Simulation_manuscript. The MATLAB programs for ScanImage for data acquisition and analysis are available at https://github.com/YaoChenLabWashU/2pFLIM_acquisition (DOI: 10.5281/zenodo.10031982).

Acknowledgements

We thank Mikhail Berezin, Hanley Chiang, and the members of Yao Chen's lab, Tim Holy's lab, and Daniel Kerschensteiner's lab for helpful feedback on the study. We thank Kerry Grens, Chao Zhou, and Erwin Arias for critical comments on the manuscript. We thank Aditi Maduska for sharing FLIM-AKAR imaging data.

Funding

U.S. National Institute of Neurological Disorders and Stroke (R01 NS119821, to YC)

Brain & Behavior Research Foundation (NARSAD Young Investigator Grant 28323, to YC)

Whitehall Foundation (2019-08-64, to YC)

McDonnell International Scholars Academy of Washington University in St. Louis (to PM)

Author Contributions

Conceptualization: PM and YC

Methodology: PM and YC

Formal Analysis: PM and YC

Writing: PM and YC

Visualization: PM

Supervision: YC

Funding Acquisition: YC

Declaration of Interests

The authors declare no competing interests.

References

1. Ma, P. *et al.* Fluorescence lifetime enables high-resolution analysis of neuromodulator dynamics across time and animals. *bioRxiv* 2022–2029; <https://doi.org/10.1101/2022.09.28.510014> (2022).
2. Lazzari-Dean, J. R., Gest, A. M. M. & Miller, E. W. Optical estimation of absolute membrane potential using fluorescence lifetime imaging. *Elife* **8**, e44522; [10.1089/bioe.2021.0007](https://doi.org/10.1089/bioe.2021.0007) (2019).
3. Brinks, D., Klein, A. J. & Cohen, A. E. Two-photon lifetime imaging of voltage indicating proteins as a probe of absolute membrane voltage. *Biophys J* **109**, 914–921; [10.1016/j.bpj.2015.07.038](https://doi.org/10.1016/j.bpj.2015.07.038) (2015).
4. van der Linden, F. H. *et al.* A turquoise fluorescence lifetime-based biosensor for quantitative imaging of intracellular calcium. *Nat Commun* **12**, 7159; [10.1038/s41467-021-27249-w](https://doi.org/10.1038/s41467-021-27249-w) (2021).
5. Zheng, K. *et al.* Time-resolved imaging reveals heterogeneous landscapes of nanomolar Ca²⁺ in neurons and astroglia. *Neuron* **88**, 277–288; [10.1016/j.neuron.2015.09.043](https://doi.org/10.1016/j.neuron.2015.09.043) (2015).
6. Chen, Y. *et al.* Endogenous Gαq-coupled neuromodulator receptors activate protein kinase A. *Neuron* **96**, 1070–1083; [10.1016/j.neuron.2017.10.023](https://doi.org/10.1016/j.neuron.2017.10.023) (2017).
7. Laviv, T. *et al.* In vivo imaging of the coupling between neuronal and CREB activity in the mouse brain. *Neuron* **105**, 799–812; [10.1016/j.neuron.2019.11.028](https://doi.org/10.1016/j.neuron.2019.11.028) (2020).
8. Mongeon, R., Venkatachalam, V. & Yellen, G. Cytosolic NADH-NAD⁺ redox visualized in brain slices by two-photon fluorescence lifetime biosensor imaging. *Antioxid Redox Signal* **25**, 553–563; [10.1089/ars.2015.6593](https://doi.org/10.1089/ars.2015.6593) (2016).
9. Yasuda, R. *et al.* Supersensitive Ras activation in dendrites and spines revealed by two-photon fluorescence lifetime imaging. *Nat Neurosci* **9**, 283–291; [10.1038/nn1635](https://doi.org/10.1038/nn1635) (2006).
10. Chen, Y., Saulnier, J. L., Yellen, G. & Sabatini, B. L. A PKA activity sensor for quantitative analysis of endogenous GPCR signaling via 2-photon FRET-FLIM imaging. *Front Pharmacol* **5**, 56; [10.3389/fphar.2016.00046](https://doi.org/10.3389/fphar.2016.00046) (2014).
11. Massengill, C. I. *et al.* Sensitive genetically encoded sensors for population and subcellular imaging of cAMP in vivo. *Nat Methods* **19**, 1461–1471; [10.1038/s41592-022-01646-5](https://doi.org/10.1038/s41592-022-01646-5) (2022).
12. Lakowicz, J. R., Szmajcinski, H. & Johnson, M. L. Calcium imaging using fluorescence lifetimes and long-wavelength probes. *J Fluoresc* **2**, 47–62; [10.1007/BF00866388](https://doi.org/10.1007/BF00866388) (1992).
13. Lee, S. J., Chen, Y., Lodder, B. & Sabatini, B. L. Monitoring behaviorally induced biochemical changes using fluorescence lifetime photometry. *Front Neurosci* **13**, 766; [10.3389/fnins.2019.00766](https://doi.org/10.3389/fnins.2019.00766) (2019).
14. Lee, S. J. *et al.* Cell-type-specific asynchronous modulation of PKA by dopamine in learning. *Nature* **590**, 451–456; [10.1038/s41586-020-03050-5](https://doi.org/10.1038/s41586-020-03050-5) (2021).
15. Yasuda, R. Imaging spatiotemporal dynamics of neuronal signaling using fluorescence resonance energy transfer and fluorescence lifetime imaging microscopy. *Curr Opin Neurobiol* **16**, 551–561; [10.1016/j.conb.2006.08.012](https://doi.org/10.1016/j.conb.2006.08.012) (2006).

16. Bastiaens, P. I. H. & Squire, A. Fluorescence lifetime imaging microscopy: spatial resolution of biochemical processes in the cell. *Trends Cell Biol* **9**, 48–52; [https://doi.org/10.1016/S0962-8924\(98\)01410-X](https://doi.org/10.1016/S0962-8924(98)01410-X) (1999).
17. Zhang, S. X. *et al.* Hypothalamic dopamine neurons motivate mating through persistent cAMP signalling. *Nature* **597**, 245–249; (2021).
18. Becker, W. Fluorescence lifetime imaging—techniques and applications. *J Microsc* **247**, 119–136; (2012).
19. Akgun, U. *et al.* Afterpulse timing and rate investigation of three different Hamamatsu Photomultiplier Tubes. *Journal of Instrumentation* **3**, T01001; [10.1088/1748-0221/3/01/T01001](https://doi.org/10.1088/1748-0221/3/01/T01001) (2008).
20. Malak, M., James, J., Grantham, J. & Ericson, M. B. Contribution of autofluorescence from intracellular proteins in multiphoton fluorescence lifetime imaging. *Sci Rep* **12**, 16584; [10.1038/s41598-022-20857-6](https://doi.org/10.1038/s41598-022-20857-6) (2022).
21. Georgakoudi, I. & Quinn, K. P. Label-Free Optical Metabolic Imaging in Cells and Tissues. *Annu Rev Biomed Eng* **25**, 413–443; [10.1146/annurev-bioeng-071516-044730](https://doi.org/10.1146/annurev-bioeng-071516-044730) (2023).
22. Raspe, M. *et al.* siFLIM: single-image frequency-domain FLIM provides fast and photon-efficient lifetime data. *Nat Methods* **13**, 501–504; [10.1038/nmeth.3836](https://doi.org/10.1038/nmeth.3836) (2016).
23. Zhang, Y. *et al.* Instant FLIM enables 4D in vivo lifetime imaging of intact and injured zebrafish and mouse brains. *Optica* **8**, 885–897; <https://doi.org/10.1364/OPTICA.426870> (2021).
24. Bowman, A. J., Huang, C., Schnitzer, M. J. & Kasevich, M. A. Wide-field fluorescence lifetime imaging of neuron spiking and subthreshold activity in vivo. *Science (1979)* **380**, 1270–1275; [10.1126/science.adf9725](https://doi.org/10.1126/science.adf9725) (2023).
25. Shcheslavskiy, V. I. *et al.* Fluorescence time-resolved macroimaging. *Opt Lett* **43**, 3152–3155; (2018).
26. Trinh, A. L. & Esposito, A. Biochemical resolving power of fluorescence lifetime imaging: untangling the roles of the instrument response function and photon-statistics. *Biomed Opt Express* **12**, 3775–3788; [10.1364/BOE.428070](https://doi.org/10.1364/BOE.428070) (2021).
27. Xiao, D. *et al.* On synthetic instrument response functions of time-correlated single-photon counting based fluorescence lifetime imaging analysis. *Front Phys* **9**, 635645; [10.1371/journal.pone.0158404](https://doi.org/10.1371/journal.pone.0158404) (2021).
28. Kumar, A. T. N. Direct Monte Carlo computation of time-resolved fluorescence in heterogeneous turbid media. *Opt Lett* **37**, 4783–4785; [10.1364/ol.37.004783](https://doi.org/10.1364/ol.37.004783) (2012).
29. Netaev, A., Schierbaum, N. & Seidl, K. Advantages and Limitations of Fluorescence Lifetime Measurements Using Single-Photon Avalanche Diode (SPAD) Array Detector: A Comprehensive Theoretical and Experimental Study. *Sensors* **22**, 3822; [10.3390/s22103822](https://doi.org/10.3390/s22103822) (2022).
30. Roethlein, C., Miettinen, M. S. & Ignatova, Z. A flexible approach to assess fluorescence decay functions in complex energy transfer systems. *BMC Biophys* **8**, 1–10; <https://doi.org/10.1186/s13628-015-0020-z> (2015).

31. Lakowicz, J. R. *Principles of fluorescence spectroscopy*. (Springer, https://doi.org/10.1007/978-0-387-46312-4_2, 2006).
32. Philip, J. & Carlsson, K. Theoretical investigation of the signal-to-noise ratio in fluorescence lifetime imaging. *JOSA A* **20**, 368–379; 10.1364/josaa.20.000368 (2003).
33. Nasser, M. & Meller, A. Lifetime-based analysis of binary fluorophores mixtures in the low photon count limit. *iScience* **25**, 10.1016/j.isci.2021.103554 (2022).
34. Köllner, M. & Wolfrum, J. How many photons are necessary for fluorescence-lifetime measurements? *Chem Phys Lett* **200**, 199–204; 10.3389/fphy.2021.647985 (1992).
35. Tilden, E. I., Maduskar, A., Oldenborg, A., Sabatini, B. L. & Chen, Y. A Cre-dependent reporter mouse for quantitative real-time imaging of Protein Kinase A activity dynamics. *bioRxiv* 2023.10.31.565028; 10.1101/2023.10.31.565028 (2023).
36. Becker, W., Su, B., Holub, O. & Weisshart, K. FLIM and FCS detection in laser-scanning microscopes: Increased efficiency by GaAsP hybrid detectors. *Microsc Res Tech* **74**, 804–811; 10.1002/jemt.20959 (2011).
37. Percie du Sert, N. *et al.* The ARRIVE guidelines 2.0: Updated guidelines for reporting animal research. *Journal of Cerebral Blood Flow & Metabolism* **40**, 1769–1777; 10.1111/bph.15193 (2020).
38. Pologruto, T. A., Sabatini, B. L. & Svoboda, K. ScanImage: flexible software for operating laser scanning microscopes. *Biomed Eng Online* **2**, 1–9; 10.1186/1475-925X-2-13 (2003).

Figure Legends

Figure 1. Procedure and analysis results of simulated fluorescence lifetime data of biosensors in brain tissue.

(A) The simulation procedure of fluorescence lifetime data. Fluorescence lifetime distribution of a FRET-based sensor was modeled as double exponential decay ($\tau_1 = 2.14$ ns, $\tau_2 = 0.69$ ns) and the lifetimes of photons were sampled with replacement. After the sensor fluorescence was convolved with instrument response function (IRF), autofluorescence (autoF) determined from brain tissue, afterpulse of the photomultiplier tube, and background fluorescence (consisting of dark current of the PMT and light leak) were added to produce final simulated data. The histograms of the final simulated data showed the same decay as experimental data. Simulation was repeated 500 times under each P_I and sensor fluorescence photon number conditions.

(B) Empirical lifetime of simulated and experimental data. autoF: autofluorescence that was empirically measured. Final simulated data include sensor fluorescence, autofluorescence, afterpulse, and background. P_I and P_2 from the fitting of experimental data were used to generate simulated data. Note that the mean of the empirical lifetime of final simulated data is not significantly different from that of experimental data. * $p < 0.05$; n.s. not significant; one-way ANOVA with Dunn's multiple comparison test.

(C) Heatmaps showing the average fitted P_I and empirical lifetime of simulated data across a range of P_I and sensor photon number conditions.

(D) Summaries of fitted P_I (left) and empirical lifetime (right) with simulated $P_I = 0.5$. * $p < 0.05$ vs sensor only; n.s. not significant vs sensor + autoF; # $p < 0.05$ vs sensor + autoF condition. Wilcoxon test.

Data are represented as mean and standard deviation.

Figure 2. Relationship between expected response amplitude and the minimum number of photons required to detect the signals.

(A-B) Minimum detectable differences of fitted P_I (A) and empirical lifetime (B) with different sensor photon numbers and with different number of pairs of sampled data (n). Data were simulated with $P_I = 0.5$.

Figure 3. Comparison of the fluorescence lifetime response by GaAsP photomultiplier tube (PMT) and hybrid detector (HBD).

(A) Gaussian IRFs used for simulation, reflecting different Gaussian widths for GaAsP PMT and HBD.

(B) Distributions of fitted P_I (left) and empirical lifetime (right) of simulated data from GaAsP PMT or HBD, with simulated $P_I = 0.5$ and showing sensor photon number dependence. Data are represented as mean and standard deviation. * $p < 0.05$, 800,000 photons vs other photon numbers. Wilcoxon test.

(C) Minimum detectable difference of fitted P_I (left) and empirical lifetime (right) with different sensor photon numbers and different numbers of data samples. Data were simulated with $P_I = 0.5$.

Figure 4. Impact of sensor photon numbers on the response amplitudes of fitted P_I and empirical lifetime.

(A, C) Distribution of fitted P_I (A) and empirical lifetime (C) from fluorescence lifetime data with simulated P_I as 0.4 and 0.5 across different sensor photon numbers. * $p < 0.05$, $P_I = 0.4$ vs $P_I = 0.5$, Wilcoxon test; # $p < 0.05$, vs photons = 800,000, Wilcoxon test.

(B, D) Distribution of the change in fitted P_I (B) and empirical lifetime (D) with different sensor photon numbers. Simulated P_I varied from 0.4 to 0.5. * $p < 0.05$, vs photon count = 800,000, Wilcoxon test.

Data are represented as mean and standard deviation.

Figure 5. Minimum sensor fluorescence needed for sensor expression-induced lifetime change to be statistically nonsignificant.

(A) Plots of change to reach statistical significance for t-tests (calculated as $1.96 \times$ standard error of the difference of the mean) and apparent lifetime change due to sensor expression. Data were simulated with $P_I = 0.5$. Each panel is plotted with a different amount of sensor expression change.

(B) Relationship between photon number changes due to expression level and the minimum number of sensor photons required not to reach statistical significance. Data were simulated with $P_I = 0.5$. The minimum numbers of sensor photons were calculated by interpolating the intersection between the two curves in (A).

Figure 2

bioRxiv preprint doi: <https://doi.org/10.1101/2023.12.20.572686>; this version posted December 21, 2023. The copyright holder for this preprint (which was not certified by peer review) is the author/funder. All rights reserved. No reuse allowed without permission.

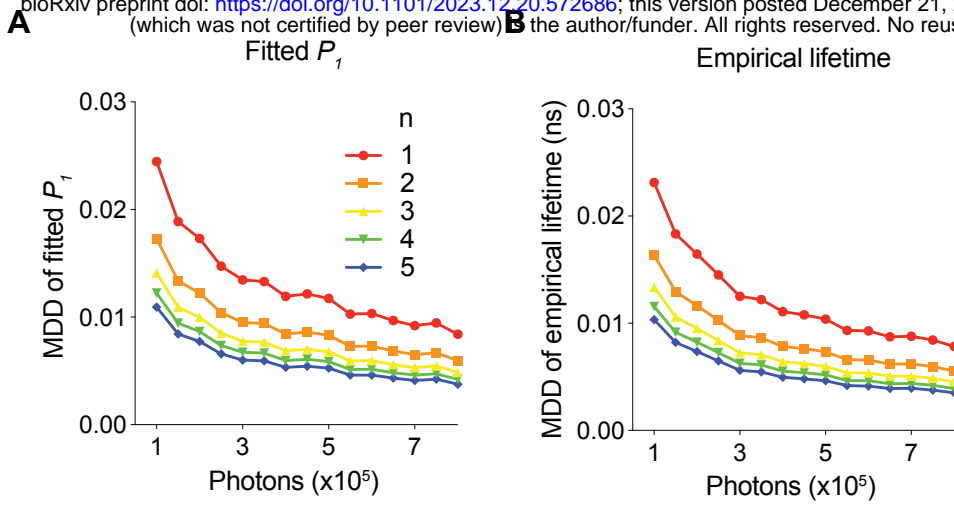


Figure 3

A bioRxiv preprint doi: <https://doi.org/10.1101/209312.20.572686>; this version posted December 21, 2023. The copyright holder for this preprint (which was not certified by peer review) is the author/funder. All rights reserved. No reuse allowed without permission.

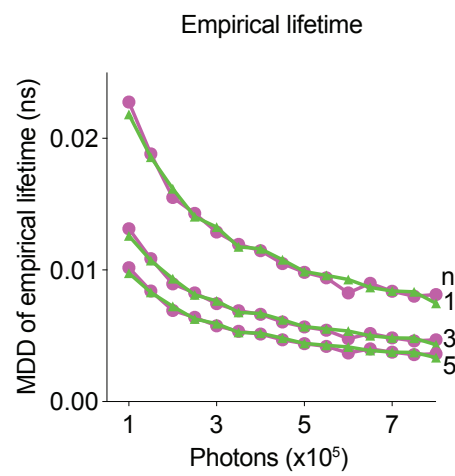
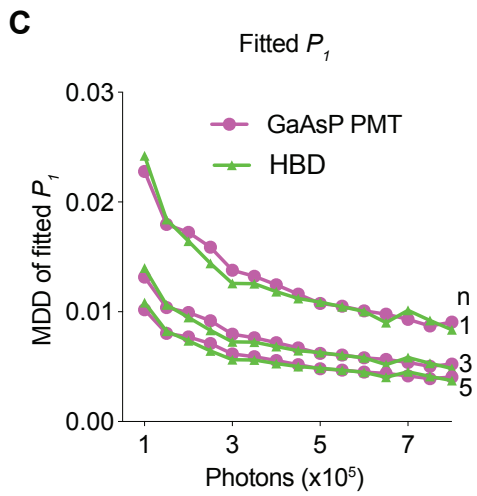
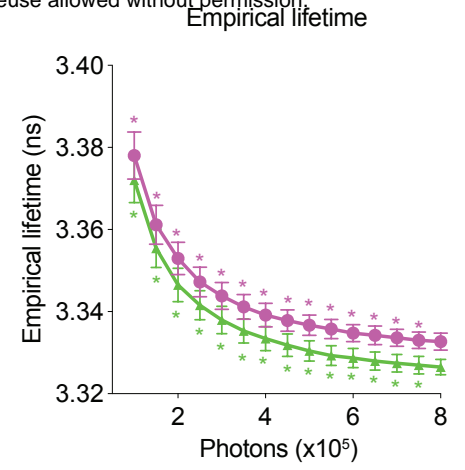
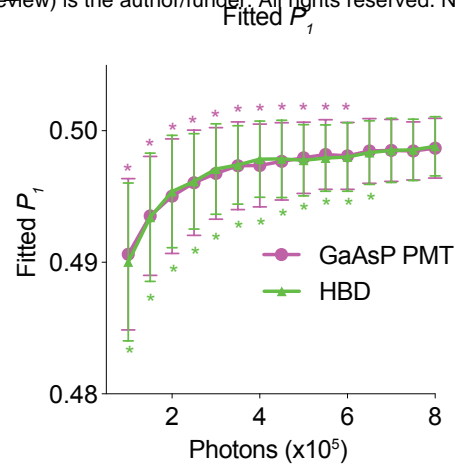
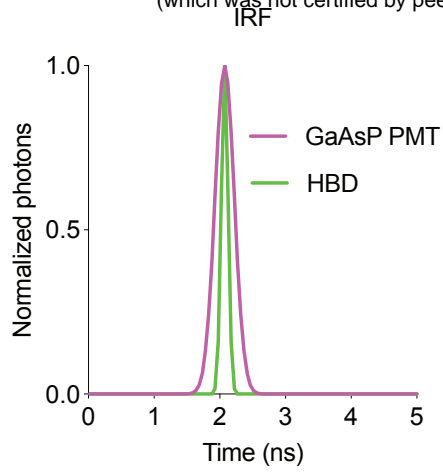


Figure 4

bioRxiv preprint doi: <https://doi.org/10.1101/2023.12.21.572686>; this version posted December 21, 2023. The copyright holder for this preprint (which was not certified by peer review) is the author/funder, who has granted bioRxiv a license to display the preprint in perpetuity. It is made available under aCC-BY-NC-ND 4.0 International license.

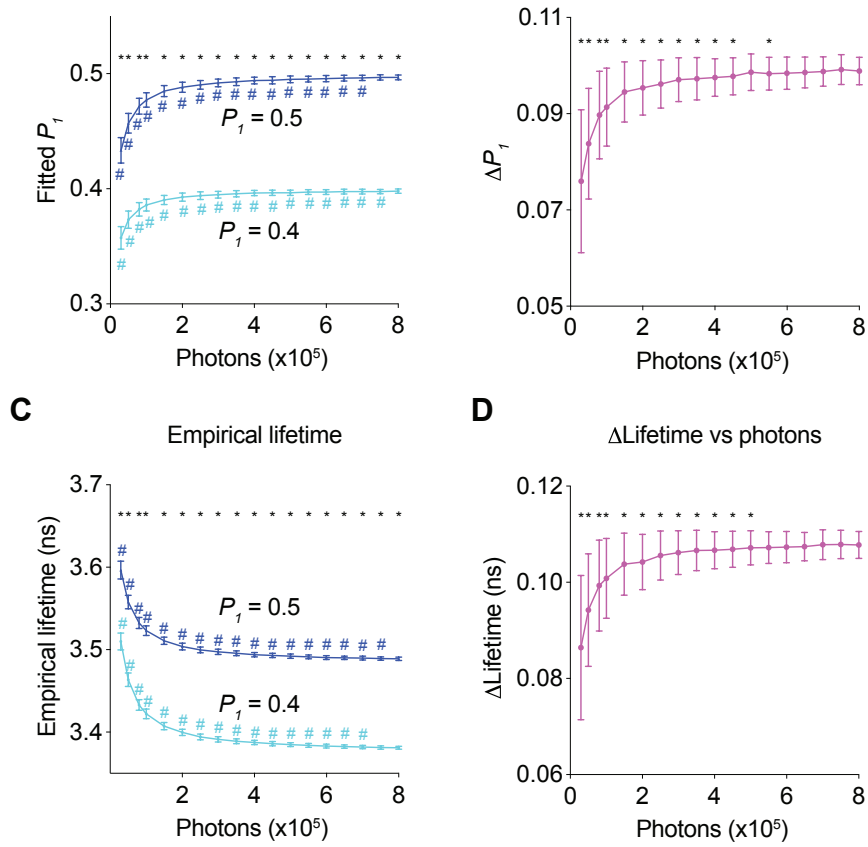


Figure 5

A bioRxiv preprint doi: <https://doi.org/10.1101/2023.12.20.572686>; this version posted December 21, 2023. The copyright holder for this preprint (which was not certified by peer review) is the author/funder. All rights reserved. No reuse allowed without permission.

